

## Original Article

# Preoperative prediction of Ki67 proliferation index obtained from non-enhanced CT measurements allows for assessing invasiveness and forecasting growth of ground-glass-opacity nodes

Hui Chen<sup>1\*</sup>, Mingjun Wan<sup>2\*</sup>, Wanbi Wang<sup>1</sup>, Hui Xing<sup>3</sup>, Feng Cao<sup>1</sup>, Guangming Li<sup>1</sup>, Guilian Yu<sup>3</sup>

<sup>1</sup>Department of Radiology, Xiangyang Central Hospital, Affiliated Hospital of Hubei University of Arts and Science, Xiangyang 441021, Hubei Province, China; <sup>2</sup>Department of Radiology, Zaoyang First People's Hospital, Zaoyang 441200, Hubei Province, China; <sup>3</sup>Department of Gynecology and Obstetrics, Xiangyang Central Hospital, Affiliated Hospital of Hubei University of Arts and Science, Xiangyang 441021, Hubei Province, China. \*Equal contributors.

Received July 29, 2016; Accepted August 30, 2016; Epub November 15, 2016; Published November 30, 2016

**Abstract:** It remains challenge to preoperatively differentiate benign or indolent nodular ground glass opacities (nGGOs) from malignant and invasive ones. In this study, we firstly established a multiple linear regression model incorporating parameters from high resolution CT for calculating the prediction of immunohistochemical Ki67 proliferation index (PI) of nGGOs based on a set of patients who had experienced operations. Namely, *Ki67-PI Prediction* =  $0.001 * TV + 0.013 * AVG + 0.028 * STD + 8.827$  (R square = 0.366,  $P < 0.001$ ), with TV, AVG and STD denoting total volume, average and standard deviation of CT attenuation of nGGOs. The noninvasive Ki67-PI Prediction showed excellent diagnostic performance in differentiating pre-invasive nGGOs from invasive ones as the actual Ki67 PI. Then, we tested this prediction model in another set of GGO patients who had not undergone surgery to confirm its prognostic value in forecasting growth of nGGOs in a 5-years follow-up period. The Ki67-PI prediction also presented excellent performance in forecasting lesions growth and volume doubling time ( $\beta = 1.002$ ,  $P < 0.001$ ). This prediction model and strategy offers a feasible method to predict the invasiveness and to forecast the growth of nGGOs from not only radiology but also pathology.

**Keywords:** Ground glass opacity, lung cancer, adenocarcinoma, Ki67, high resolution computed tomography

## Introduction

In recent years, nodular ground glass opacities (nGGOs) have raised widespread concerns because of increasing frequency due to the introduction of low-dose computed tomography (CT) to lung cancer screening for nGGOs [1-3]. Although the recommendations for management of subsolid nodes had been proposed by the Fleischner Society, the diagnostic standard to define which lesion necessitate treatment and the optimal management strategy to a specific node remain controversial [4, 5].

Since the International Association for the Study of Lung Cancer (IASLC), the American Thoracic Society (ATS), and the European Respiratory Society (ERS) have proposed a new multidisciplinary classification of lung adeno-

carcinoma in 2011, pathological differentiation of GGO has become imperative for thoracic surgeons, as complete resection of pre-invasive and minimally-invasive adenocarcinoma contributed to 100% 5-year disease-free survival [6, 7]. It has been described that the natural development of GGO tumor follows a multi-step progression from atypical adenomatous hyperplasia (AAH) to adenocarcinoma in situ (AIS), to minimally invasive adenocarcinoma (MIA), and finally to invasive adenocarcinoma (IAC) [7, 8]. Many CT characteristics of nGGOs have been identified indicating lesions' malignancy and prognosis, such as the diameter, volume, mass, attenuation and heterogeneity, etc [3, 9-11]. The presentations and measurements of nGGOs on CT significantly correlate with the pattern and extent of lepidic growth on pathol-

## Ki67-PI prediction allows assessing invasiveness and forecasting growth of GGO

**Table 1.** Demographic, radiological and pathological characteristics of nGGOs from group-A patients (n = 189)

Variables	PIA	IA	P1	Ki67 PI (%)	P2
Gender			0.132*		0.895§
Male	38	69		5.99 ± 3.25	
Female	38	44		5.93 ± 3.45	
Age (year)	51.05 ± 8.01	52.64 ± 8.08	0.186§		
GGO type			< 0.001*		< 0.001§
Pure	35	19		4.58 ± 3.13	
Mix	40	94		6.53 ± 3.25	
Shape			0.230*		0.029#
Round	35	36		5.06 ± 3.46	
Oval	19	32		6.26 ± 3.01	
Polygonal	12	22		6.73 ± 3.01	
Irregular	10	23		6.66 ± 3.50	
Margin			0.066*		0.144#
Smooth	25	19		5.09 ± 3.26	
Lobulated	12	18		6.35 ± 2.86	
Spiculated	28	51		5.94 ± 3.42	
Lobulated and spiculated	11	25		6.74 ± 3.45	
Tumor-lung interface			0.109*		0.166§
Well defined	30	58		6.32 ± 3.36	
Ill defined	46	55		5.65 ± 3.29	
Location			0.281*		0.133#
LUL	15	35		6.72 ± 3.03	
LLL	8	9		5.62 ± 4.45	
RUL	34	48		5.96 ± 3.29	
RML	8	13		5.84 ± 3.59	
RLL	11	8		4.40 ± 2.42	
CT measurements					
Diameter (mm)	11.06 ± 4.55	16.12 ± 4.33	< 0.001§		
TV (mm <sup>3</sup> )	392.51 ± 429.35	992.22 ± 771.74	< 0.001§		
MAX (HU)	-193.97 ± 177.35	92.44 ± 219.43	< 0.001§		
AVG	-550.38 ± 42.21	-497.25 ± 61.44	< 0.001§		
STD	73.96 ± 23.18	134.51 ± 36.21	< 0.001§		
Ki67 PI (%)	3.14 ± 2.07	7.86 ± 2.59	< 0.001§		
Prediction of Ki67 PI (%)	4.14 ± 0.94	7.12 ± 1.55	< 0.001§		

Note: PIA, preinvasive adenocarcinoma, including atypical adenomatous hyperplasia (AAH) and adenocarcinoma in situ (AIS); IA, invasive adenocarcinoma, including minimally invasive adenocarcinoma; LUL, left upper lobe; LLL, left lower lobe; RUL, right upper lobe; RML, right median lobe; RLL, right lower lobe; TV, total volume; MAX, AVG and STD denotes maximal, average and standard deviation of CT attenuation within ground-glass-opacity nodes; HU, Hounsfield unit; PI, proliferation index. Unless otherwise indicated, numerical variables were recorded as mean ± standard deviation. P1 indicates difference significance of variables between PIA and IA, while P2 indicates difference significance among levels of categorical variables. \*, Chi square test; §, Student t test; #, One way ANOVA analysis.

ogy [6, 12]. However, it remains challenge for clinicians to differentiate benign or indolent nGGO from malignant and invasive one.

Understanding pathological-radiological inter-relationship of nGGO has led to changes in diagnostic and therapeutic strategies [13].

## Ki67-PI prediction allows assessing invasiveness and forecasting growth of GGO

Therefore, it is necessary to develop a prediction model that can reflect both the histopathological features and the radiological characteristics of invasive nGGOs to identify the optimal target population for treatment.

Proliferation of tumor cells is an important pathological feature of lung cancer. A nuclear antigen named Ki67 has demonstrated roles in tumorigenesis, as increased Ki67 expression is closely correlated with the proliferation and invasiveness of tumors cells [14]. Based on immunohistochemical assessment of this antigen, many studies have demonstrated that the proliferative activities determined by Ki67 correlated with the prognosis of patients with lung cancer [14-17]. Even more interesting is the result in study by Peng et al [17] that the prediction of Ki67 labeling index which was calculated from preoperative non-enhanced CT measurements of nGGOs showed reliable values in predicting pathological status and invasiveness of nGGOs. However, the authors only provided a “discovery screen” for predicting Ki67 expression, but had not tested it in “prognosis screen” to confirm it.

In this study, we firstly established a prediction model of Ki67 proliferation index (PI) incorporating parameters from CT image with immunohistochemical Ki67 expression of nGGOs based on a set of patients who had experienced operations as done by Peng et al [17]. Then we tested the prognostic value of this model in another set of GGO patients who had not undergone surgery.

### Materials and methods

#### *Patient selection and follow-up strategy*

This study was approved by the institutional review board of our hospital. Informed consents were obtained from all subjects included in this study.

Firstly, we included 189 patients (group A) with nGGOs on high resolution CT (HRCT) that had been resected completely in our hospital from January 2010 to December 2014 to establish Ki67 prediction model. The inclusion criteria were: 1) nGGOs were found on HRCT; 2) only one GGO was observed in each patient; 3) the maximum diameters of nGGOs were 5 mm-3 cm; 4) percentages of GGO content were 50%

or more; 5) pathological diagnosis of lesions were adenocarcinoma. Patients that met any of the follows were excluded: 1) without pathological diagnosis; 2) preoperative CT was performed in other hospital; 3) with radio-chemotherapy or biopsy preoperatively, 4) the CT images were 2.0-mm or more in thickness or reconstructed without a lung algorithm. Pathological diagnoses included AAH (n = 30), AIS (n = 46), MIA (n = 65) and IAC (n = 38). For statistical analysis, AAH and AIS were classified into preinvasive adenocarcinoma (PIA) while MIA and IAC were classified into invasive adenocarcinoma (IA) because of similar biological behavior. **Table 1** shows the clinical, radiological and pathological characteristics of these patients.

Then, another set of 63 patients (group B) with nGGOs were selected for testing the prediction model, with the same enrollment criteria as group A except pathological diagnosis. Serial follow-up CT examinations lasting 5 years at most were performed to these patients in accordance to the following strategy: the first year, once every 2 months; the second to third year, once every 3 months; and the fourth to fifth year, once every 6 months. We closed the follow-up work when patient met anyone of the follows: 1) lesions' volumes doubled, 2) imperative operations were done, 3) came to the end of the 5-years period, 4) lost to follow up, 5) died before the close of follow up.

#### *CT Acquisition*

The chest CT scans were performed from the lung apices to the bases with scanners of Somatom Sensation 16 (Siemens Healthcare, Forchheim, Germany). The scanning parameters were 120 kV, 100 mAs, collimation configuration of 16×1.5 mm, pitch of 1.25 and exposure of 0.5 s per rotation. For the follow-up of group-B patients, target scanning focused on lesions with standard dose were performed. Raw data were reconstructed for HRCT with thickness of 1.5 mm, interval of 0.75 mm and a sharp kernel algorithm (B70f) for reconstruction of lung. Window settings were performed on all images to optimally assess lung parenchyma (window level, -600 Hounsfield units [HU]; window width, 1200 HU) and mediastinum (window level, 40 HU; window width, 400 HU).

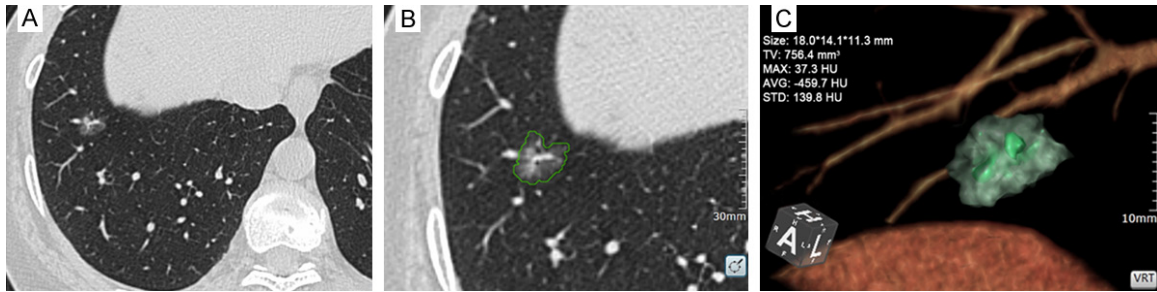


**Figure 1.** Three-dimensional processing and measuring of a typical GGO node. A. Transversal high resolution CT (HRCT) shows a mix-type GGO lesion located in right lower lobe of the lung. B. A transversal image of HRCT showing manually delineating the outline of this lesion. C. Volume rendering technique (VRT) image generated automatically by the software with the lesion marked in green color and the relative measurements of the lesion listed in the left up corner, including size, total volume (TV), as well as maximum (MAX), average (AVG) and standard deviation (STD) of CT attenuation.

#### *Radiological evaluation of lesions*

Two radiologists of 9 and 7 years experiences respectively evaluated the CT images, blinding to patients' demographic information. For all initial CT imaging, lesion's location, shape, tumor-lung interface, and margin were assessed, and the diameters, total volume (TV), maximum (MAX), average (AVG) and standard deviation (STD) of CT attenuations of the total nGGO were measured. According to recommendation of the Nomenclature Committee of the Fleischner Society, GGO is defined as a hazy opacity that does not obscure the underlying bronchial structures or pulmonary vessels [18]. The nGGOs were classified into pure GGO and mix GGO with the latter consisting of solid component as well. Round, oval, polygonal, or irregular were used to describe the shape of nGGOs. Lesions' margins were described as smooth, lobulated, spiculated, or lobulated with spiculation. Tumor-lung interface was recorded as well- or ill-demarcated. The diameter was the maximal dimension on transversal images. TV, MAX, AVG and STD were measured by drawing and summing a series of regions of interest (ROIs) on continuous transversal images covering as large an area as possible of the whole lesion but excluding large vessels, until the entire lesion was covered (**Figure 1**).

For the follow-up evaluation, only the diameter, TV and AVG were measured. Based on these measurements, lesions were defined as stable or growing, with growth being defined as: attenuation increases of at least 30 HU and (or) diameter increases by at least 20% in node  $\geq$

10 mm, 30% in nodules of 5-9 mm [19, 20]. For growing nGGO, the doubling time (DT) of volume was recorded in unit of month, which was defined as the time interval between the initial CT scan and the last CT scan when lesion's volume increased to twice or more of the initial one.

#### *Histopathological diagnosis and Ki67 evaluation of lesions in patients from group A*

The paraffin-embedded specimens from group-A patients were retrieved, cut for tissue sections and then stained with hematoxylin and eosin (HE) for pathological diagnosis by two experienced lung pathologists. Immunohistochemical staining was performed on the sections with monoclonal anti-Ki67 antibody (Abcam 92742, Cambridge, MA, USA; 1:100 dilution) to the Ki67 antigen based on the established methodology [17]. Ki67-positive nucleus were stained brown. An Olympus BX 50 microscope equipped with a cannon camera (Power Shot A80, Tokyo, Japan) was used for microscopy and image capturing. Percentages of positive cells were quantitatively calculated by using Image Pro Plus 6.0 (Media Cybernetics, Washington DC, USA; **Figure 2**). This software and technique has been widely used in biomedicine, which had showed favorable reliability [17, 21, 22].

#### *Statistical analysis*

Inter-observer agreement between the two observers were analyzed by calculating intra-class correlation coefficients (ICCs) for numerical variables and by Cohen *Kappa* test for cat-

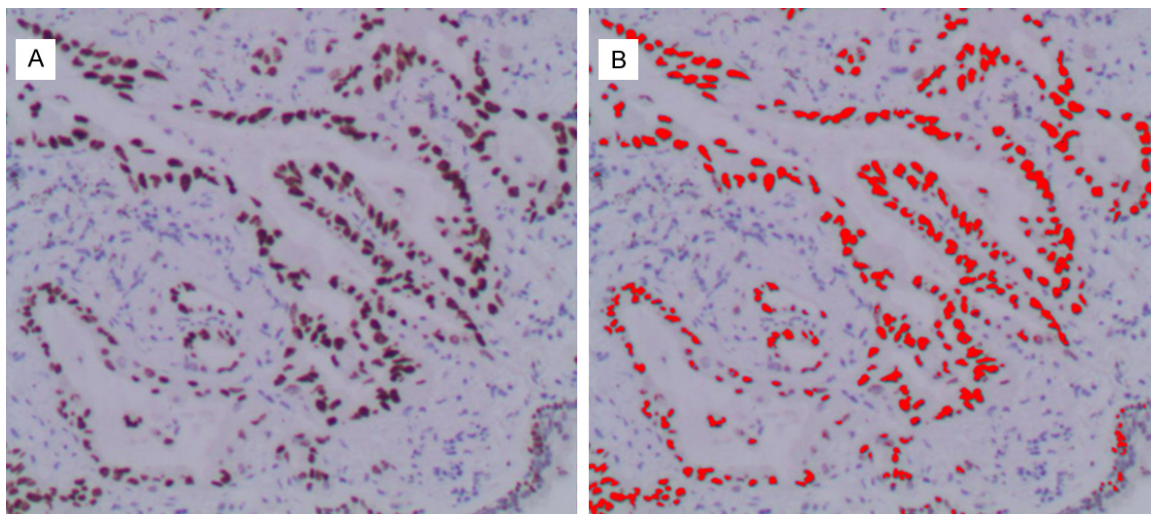


**Figure 2.** Representative photomicrographs of immunohistochemical detection and measurement of Ki67 proliferation index (PI). A. The immunohistochemical image of Ki67 staining (magnification  $\times 200$ ) with positive expression of Ki67 presented as tan particles located in nucleus of tumor cells. B. Quantitative measurement of Ki67 PI by Image Pro Plus 6.0 (red areas denote detection of the software).

**Table 2.** Inter-observer agreement in nGGOs evaluation on high resolution CT

Variables	ICC/Kappa	95% CI
Type	0.824	0.711-0.902
Shape	0.716*	0.635-0.838
Margin	0.757*	0.649-0.852
Tumor-lung interface	0.745*	0.634-0.841
Location	1.000*	1.000-1.000
Diameter (mm)	0.876	0.804-0.937
Total volume (TV) (mm <sup>3</sup> )	0.881	0.767-0.938
Maximum CT attenuation (Max) (HU)	0.835	0.686-0.915
Mean CT attenuation (Mean) (HU)	0.889	0.832-0.931
STD of CT attenuation	0.914	0.826-0.947

Note: Kappa-value  $\leq 0.4$  indicates poor agreement; 0.41-0.60 moderate agreement; 0.61-0.80 good agreement; and  $\geq 0.81$  excellent agreement. ICC, intra-class coefficient. CI, confidence interval. \*, weighted Kappa.

egorical variables. An ICC greater than 0.75 indicates good agreement [23]. The Kappa-value  $\leq 0.4$  indicates poor agreement; 0.41-0.60 moderate agreement; 0.61-0.80 good agreement; and  $\geq 0.81$  excellent agreement [24]. The averages of numerical variables measured by the two reviewers were used for further analysis, while consensus were achieved by negotiation for categorical variables if necessary.

Numerical variables were expressed as mean  $\pm$  standard deviation (SD), while categorical

variables were expressed as frequencies or percentages. Chi-square or Fisher's exact tests were used to analyze intergroup differences of categorical variables. The student t test and One-way ANOVA analysis were used appropriately for analyzing intergroup differences of numerical variables. Univariate correlation analyses and partial correlation analyses were performed to investigate associations between radiological characteristics and Ki67 PI of nGGOs. Crude and adjusted effects (beta coefficients) were estimated. Multivariate stepwise linear regression was conducted to identify independent variables that predicting Ki67 PI, and to establish equation for calculating Ki67-PI Prediction. Finally, the receiver operating characteristic (ROC) curve analy-

ses were performed for comparing capacity of numerical variables in predicting invasiveness and growth of nGGOs, and the multivariate Cox regression analysis was conducted to identify independent variables that could predict lesions' DT. Differences of diagnostic performance were analyzed between Ki67 PI and Ki67-PI Prediction by comparing area under curves (AUCs) according to method described by DeLong et al [25]. All statistical analyses were performed using SPSS 20 (IBM SPSS Inc., Chicago, IL, USA), with a two sided *P* value less than 0.05 indicating statistical significance.

## Ki67-PI prediction allows assessing invasiveness and forecasting growth of GGO

**Table 3.** Univariate analysis for the relationships between numerical variables and Ki67 proliferation index

Variables	Mean	SD	B coefficient	P value	Adjusted $\beta$ coefficient	P value
Diameter (mm)	14.09	4.78	0.463	< 0.001	0.227	0.126
TV (mm <sup>3</sup> )	751.07	743.36	0.394	< 0.001	0.107	0.002
MAX (HU)	-22.72	293.27	0.504	< 0.001	0.274	< 0.001
AVG (HU)	-518.61	53.43	0.372	< 0.001	0.200	0.006
STD	110.16	49.48	0.516	< 0.001	0.283	< 0.001

Note: SD, standard deviation; TV, total volume; MAX, maximum CT attenuation; AVG, average CT attenuation; STD, standard deviation of CT attenuation.

### Results

#### Demographic and radiological information of patients in group A

Of the patients in group A, 107 (56.7%) were male and 82 (43.3%) were female, with a mean age of 52.0 years (SD, 8.07; range, 28-72 years). Seventy six (40.2%) nGGOs were pathologically classified into PIA, including 30 (15.9%) AAH and 46 (24.3%) AIS, while 113 (59.8%) lesions were IA consisting of 74 (39.2%) MIA and 39 (20.6%) IAC. There was no significant difference in sex ratio or age distribution between PIA and IA lesions ( $P = 0.132$  and  $0.186$ , respectively; **Table 1**).

#### Radiological features of nGGOs from group-A patients

The inter-observer agreement in evaluating categorical characteristics of nGGOs are good to excellent, with the *Kappa* values ranging from 0.716 for nodular shape to 1.000 for lesions' location (**Table 2**). For CT measurements, the calculated inter-observer ICCs were also excellent, which ranged from 0.835 for MAX to 0.914 for STD (**Table 2**).

Significantly more mix-type nGGOs were found to be IAs pathologically, as compared to the PIA lesions, with  $P$  values < 0.001, while the other morphological features of lesions including the shape, margin, tumor-lung interface and location were homogeneously distributed between PIA and IA lesions ( $P$  values all > 0.05; **Table 1**). CT measurements of nGGOs regarding diameter, TV, MAX, AVG and STD showed significant inter-group differences between PIA and IA lesions, with  $P$ -values all < 0.001. IA lesions showed significantly larger diameter and TV, as well as higher MAX, AVG and STD than PIA

lesions, ( $P$ -values all < 0.001; **Table 1**).

#### Correlations of Ki67 PI and CT characteristics of nGGOs

The mean Ki67 PI of PIA and IA lesions were  $3.14 \pm 2.07$  and  $7.86 \pm 2.59$ , respectively, with significant inter-group differences ( $P < 0.001$ ; **Table 1**). GGO type and shape

showed significant intergroup differences of Ki67 PI, with  $P$  values being < 0.001 and = 0.029, respectively (**Table 1**). The other categorical variables regarding patient gender, lesions' margin, tumor-lung interface and location were identified possessing insignificant intergroup differences of Ki67 PI ( $P$  all > 0.05, **Table 1**). Univariate analysis revealed that TV, MAX, AVG, and STD were significantly correlated with Ki67 PI, either before or after adjusted by other covariates, as shown in **Table 3**. The adjusted  $\beta$  coefficient of Diameter was not statistically significant ( $P = 0.126$ ). This means it may have colinearity with other variables such as the TV. We precluded GGO shape from final regression analysis because of its inefficiency in differentiating IA lesions from the PIA ones ( $P = 0.230$ , **Table 1**).

Finally, GGO type, TV, MAX, AVG, and STD were selected for multivariate linear stepwise regression to investigate their relationships with Ki67 PI, quantitatively. As shown in **Table 4**, TV, AVG and STD were independent variables predicting Ki67 PI ( $P$  values all < 0.001), of which STD presented the largest standardized  $\beta$ -coefficient (0.368) indicating the largest power in prediction of Ki67 PI. However, GGO type and MAX were excluded from the final model, which means they might be not independent factors predicting Ki67 PI. Consequently, an equation for calculating Ki67-PI Prediction were established based on these independent variables (TV, AVG and STD) as follows:

$$\text{Ki67-PI Prediction} = 0.001 * \text{TV} + 0.013 * \text{AVG} + 0.028 * \text{STD} + 8.827 \text{ (R square} = 0.366, P < 0.001).$$

The Ki67-PI Prediction were calculated as  $7.12 \pm 1.55$  for IA lesions, which were significantly higher than PIA lesions ( $4.14 \pm 0.94$ ,  $P < 0.001$ ;

**Table 4.** Multivariate stepwise linear regression analysis (dependent variable: Ki67 proliferation index)

Variables	Unstandardized $\beta$ -coefficients	SE	Standardized $\beta$ -coefficients	P-value
TV	0.001	0.0003	0.223	0.001
AVG	0.013	0.0034	0.236	< 0.001
STD	0.028	0.0050	0.368	< 0.001
Constant	8.827	1.9646	NA	< 0.001

Note: Gender and MAX (maximal CT attenuation) was excluded from the final model. TV, total volume; AVG, average CT attenuation; STD, standard deviation of CT attenuation. SE, standard error. NA, not associated.

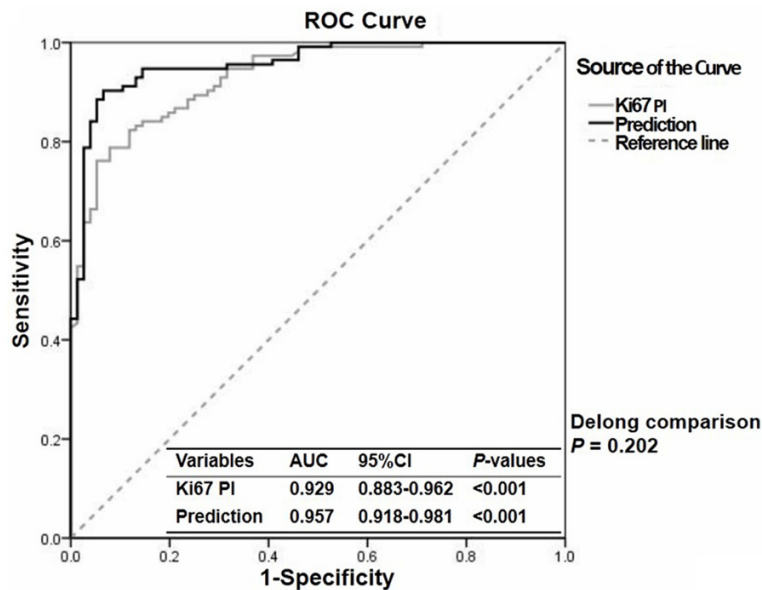


**Figure 3.** Receiver operating characteristic (ROC) curve analysis of Ki67-PI Prediction and the actual Ki67 PI for comparison in differentiating IA lesions from PIA ones. Areas under the curve (AUCs) of Ki67-PI Prediction were higher than the actually measured one, although not statistically significant (AUC 0.957 vs. 0.929,  $P = 0.202$ ) compared by method described by Delong et al.

**Table 1).** Furthermore, we compared the diagnostic performance of Ki67-PI Prediction with the actual one by comparing their AUCs (**Figure 3**). The Ki67 PI prediction even had a little larger AUC in differentiating IA lesions from PIA ones (AUC 0.957 vs. 0.929,  $P = 0.202$ ; **Figure 3**), although not statistically significant. The optimal threshold of Ki67-PI Prediction for differentiating IAs from PIAs was 5.37%, with corresponding sensitivity and specificity being 90.3% and 93.4%, respectively.

*Follow-up, demographic and radiological characteristics of patients in group B*

Of the 63 patients enrolled for following up, 11 (17.5%) cases were censored because of imper-

ative operation ( $n = 6$ , 9.5%), lost in follow-up ( $n = 3$ , 4.8%) and death ( $n = 2$ , 3.2%). Finally, 52 patients were successfully followed up, with a follow-up rate of 82.5%. Twenty nGGOs (31.7%) were stable during the 5-years period, while 35 (55.6%) lesions presented a growing pattern. Of the 35 patients with growing nGGOs, 3 cases were closed to follow up before the end of the 5-years period because of imperative operation ( $n = 2$ ) and death ( $n = 1$ ). Two cases failed to identify the time point of doubled volumes. Eventually, 30 nGGOs presented doubling volumes during the period of follow up, with the doubling time being  $27.45 \pm 15.50$  (**Table 5**). The follow up of the 63 patients were shown in **Figure 4**.

In patients from group B, 33 (60.0%) were male and 22 (40.0%) were female, with age ranging from 36 to 79 years old (mean  $\pm$  SD,  $52.7 \pm 7.89$ ). There was no significant difference in sex ratio or age distribution between stable and growing lesions ( $P = 0.567$  and 0.893, respectively; **Table 1**). The growing lesions presented significantly larger initial diameter and TV, as

well as higher initial AVG and STD than the stable ones, with  $P$ -values being all less than 0.05, but initial MAX was not significantly different between IA and PIA lesions ( $P = 0.062$ , **Table 5**). ROC analysis showed the AUCs of lesions' initial Diameter, TV, MAX, AVG, STD and Ki67-PI Prediction were 0.694, 0.740, 0.657, 0.761, 0.894 and 0.927, respectively to predicting lesions growth (**Figure 5**). Obviously, the Ki67-PI Prediction owned the best prediction performance.

In addition, we performed Cox regression analysis to identify relationships between initial CT characteristics of nGGOs and their volume-doubling time obtained during the follow-up period. Because of obvious colinearities between TV,

## Ki67-PI prediction allows assessing invasiveness and forecasting growth of GGO

**Table 5.** Demographic, radiological and follow-up information of nGGOs from group-B patients (n = 55)

Variables	Stable	Growing	P
Gender			0.567*
Male	12	21	
Female	8	14	
Age (year)	52.40 ± 7.83	52.71 ± 8.54	0.893§
Initial CT measurements			
Diameter (mm)	12.15 ± 4.78	15.91 ± 6.11	0.022§
TV (mm <sup>3</sup> )	423.41 ± 401.48	1186.66 ± 1035.35	0.003§
MAX (HU)	-116.60 ± 161.65	7.55 ± 263.67	0.062§
AVG	-556.65 ± 40.29	-508.34 ± 56.16	< 0.001§
STD	72.20 ± 26.81	134.98 ± 42.49	0.001§
Ki67 PI prediction (%)	4.04 ± 1.07	7.18 ± 1.96	< 0.001§
Volume-doubled lesions	0	30	
Doubling time (month)	NA	27.45 ± 15.50	

Note: PIA, preinvasive adenocarcinoma, including atypical adenomatous hyperplasia (AAH) and adenocarcinoma in situ (AIS); IA, invasive adenocarcinoma, including minimally invasive adenocarcinoma; LUL, left upper lobe; LLL, left lower lobe; RUL, right upper lobe; RML, right median lobe; RLL, right lower lobe; TV, total volume; MAX, AVG and STD denotes maximal, average and standard deviation of CT attenuation within ground-glass-opacity nodes; HU, Hounsfield unit; PI, proliferation index. Unless otherwise indicated, numerical variables were recorded as mean ± standard deviation. P1 indicates difference significance of variables between PIA and IA, while P2 indicates difference significance among levels of categorical variables. \*, Chi square test; §, Student t test. NA, not associated.

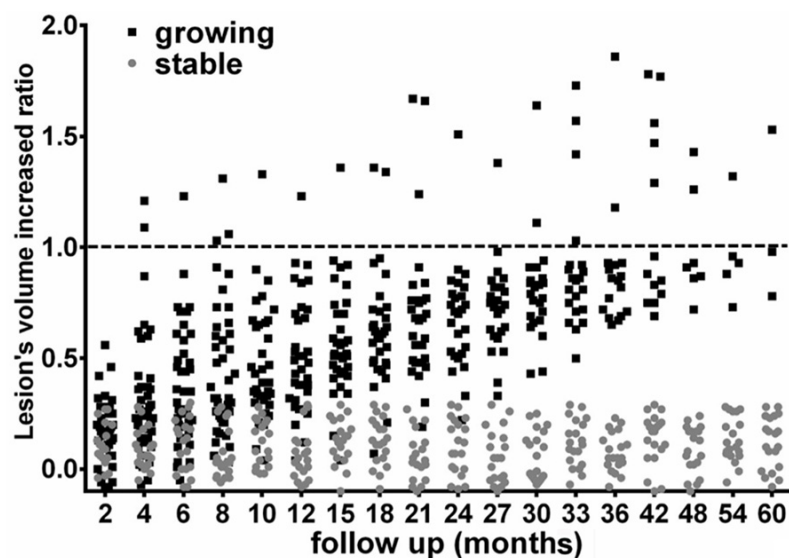


**Figure 4.** The follow up of the 63 patients in group B showing changes in size of lesions within the 5-years period. The lesions volume increase ratio was calculated as: (follow-up volume-initial volume)/initial volume. The yellow line divides lesions with doubled volumes from those without during the 5-years follow up.

AVG, STD and Ki67-PI Prediction, we excluded TV, AVG and STD from the regression model beforehand. Final results were shown in **Table**

and STD, and commonly present as mix GGOs or come up to be solid nodes with increased diameters and TVs [6, 17, 29]. In this study,

**6.** Only Ki67-PI Prediction was the independent variables that could forecast doubling time of growing nGGOs ( $\beta = 1.002$ ,  $P < 0.001$ ). In lesions with similar characteristics with respect to the variables analyzed, a 1% increase of Ki67-PI Prediction forecasts a 2.732-fold increase of probability that nGGOs would doubled in volume within 5 years.

### Discussion

Advances in imaging technology has promoted a more precise and quantitative pattern in assessing nGGOs than traditional one-dimensional or two-dimensional methods [9, 26, 27]. As GGO lesions not always grow in a homogeneous way and no clear dividing lines exist between GGO lesions of different pathological status, quantitative analysis of GGO lesions seems more accurate and reasonable. In recent years, many hallmarks of nGGOs obtained from quantitative CT that indicates tumor invasiveness have been identified [6, 10, 28, 29]. The radiological characteristics of nGGOs present a continuous progression that may be parallel to the pathological advance from pre-invasive (including AAH and AIS) to invasive status (including MIA and IAC). For instance, pre-invasive nGGOs most likely own a low MAX, AVG and STD, while invasive lesions generally own higher MAX, AVG

## Ki67-PI prediction allows assessing invasiveness and forecasting growth of GGO

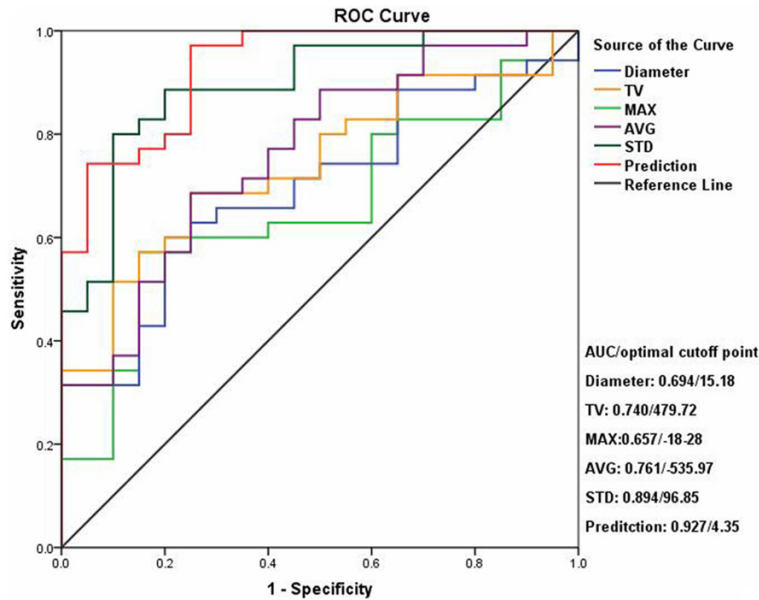


**Figure 5.** Receiver operating characteristic (ROC) curve analysis of initial CT measurements of nGGOs as well as Ki67-PI Prediction in forecasting lesions growth during the follow-up period. According to area under the curve (AUC) of all variables, Ki67-PI Prediction presented a better predicting performance than other variables. TV, total volume; MAX, AVG and STD denote, in order, the maximum, average and standard deviation of CT attenuation within nGGOs.

**Table 6.** Multivariate Cox regression analysis (dependent variable: Doubling time)

Variables	$\beta$ -coefficients	SE	Wald	HR (exp ( $\beta$ ))	P-value
Gender	0.265	0.405	0.427	1.303	0.513
Age	0.001	0.024	0.001	1.001	0.977
Ki67 PI Prediction	1.002	0.188	28.248	2.723	< 0.001
Diameter	0.046	0.045	1.052	1.047	0.305
MAX	-0.002	0.001	5.419	0.998	0.056
Type	-0.109	0.472	0.053	0.897	0.818

Note: MAX, maximum CT attenuation; SE, standard error; HR, hazard ratio.

Diameter, TV, AVG and STD were also identified significantly increased from PIA and IA lesions. Diameter and TV characterize GGO from the perspective of whole basic framework of proliferation in comparison to AVG which describe its substantiality and internality. STD manifests degree of heterogeneity within the whole node.

However, all of these quantitative CT measurements are preoperative which cannot directly reflect lesions' pathology per se. Since the new multidisciplinary classification of lung adenocarcinoma had been proposed by IASLC/ATS/ERS in 2011, pathological differentiation of

nGGOs has been imperative and attractive for thoracic surgeons, as complete resection of pre-invasive and minimally-invasive adenocarcinoma contributes to 100% 5-year disease-free survival [6, 7]. Proliferation is a key feature of progressing lung cancer, in which the nucleus antigen-Ki67-is highly expressed. Peng et al [17] investigated an immunohistochemical index, namely Ki67 LI, for assessing invasiveness of nGGOs. Based on ROC analysis, this index showed good diagnostic performance either in differentiating MIA from PIA, or in distinguishing IAC from MIA. Similar in this study, the Ki67 PI also showed excellent diagnostic performance in differentiating IAs from PIAs based on ROC analysis (AUC = 0.929,  $P < 0.001$ ). The high expression of Ki67 in invasive lesions indirectly reflects undue proliferation of malignant tumors, which may associated with its critical role in cell cycle progression [14, 30]. The Ki67 protein is present during all active phases of the cell cycle (G1, S, G2, and mitosis), but is absent from resting cells (G0) [30]. This makes it an excellent marker for determining the growth fraction of a given

cell population for quantitatively assessing proliferation of tumor tissue.

Inadequacy is that immunohistochemical diagnosis of pulmonary nodeis always invasive either from surgery or biopsy. Only if there is a pathological index that can be quantitatively predicted preoperatively, can we accurately judge pathological features of nGGOs. As we know, the increasing expression of Ki67 goes along with the invasive progression of tumor cells, leading to a larger and more substantial parenchyma involved resulting in larger size and higher CT attenuation on HRCT. However,

## Ki67-PI prediction allows assessing invasiveness and forecasting growth of GGO

the tumor cells that in high proliferation will not always grow in a consistent step but commonly scattered in involved lung parenchyma, which will lead to higher STD of CT attenuation within nodes. In study of Peng et al [17], positive relationships had already been identified between CT characteristic of nGGOs and lesions' immunohistochemical Ki67 labelling index. Similar in current study, all CT measurements presented significant positive correlations with Ki67 PI. Thus, it is feasible to associate lesions' Ki67 PI from histopathology with corresponding parameters from HRCT. In current study, we established a multivariable linear regression equation to preoperatively predict the Ki67 PI of nGGOs based on measurements from HRCT. The prediction of Ki67 even showed a little higher diagnostic performance in differentiating IA lesions from PIA ones, compared to the actual Ki67 PI from immunohistochemistry, although not statistically significant. Peng et al [17] even revealed that the Ki67 PI Prediction not only presented excellent performance in differentiating IA lesions from PIA ones, but also showed good performance in distinguishing IACs from MIAs. Consequently, we considered that the correlations between CT parameters and Ki67 PI, and the regression model for calculating Ki67-PI Prediction are biological and physiological more than just statistical or mathematical.

The term GGO, as detected in the lung parenchyma on HRCT, is defined as "hazy increased attenuation in the lung that does not obliterate the bronchial or vascular margins" by the Fleischner Society [18]. This definition is non-specific and does not necessarily reflect the pathological etiology of GGO nodes. A variety of benign and malignant diseases have been reported presenting as GGO on HRCT, including pulmonary edema, pulmonary alveolar proteinosis, alveolar hemorrhage, nonspecific interstitial pneumonia, hypersensitivity pneumonitis, sarcoidosis, noncaseating granulomatous deposition, and adenocarcinoma [31, 32]. It is reported that only 34% of the nGGOs detected were confirmed malignant [33]. Furthermore, some of the nGGOs showed an indolent growing pattern. Koo et al reported that about 52% of the GGO lesions presented a slow rate of growth of less than 2 mm per year [34]. Similar in this study, about 54.5% (30/55) of the total followed-up nGGOs were stable during the

5-year period, and even for growing GGO nodes, the volume doubling time were also not short ( $27.45 \pm 15.50$  months). Thus, it is important to differentiate benign or indolent nGGO from malignant and invasive one before operation, in order to avoid unnecessary surgery. In current study, the calculated prediction of Ki67 PI based on initial CT measurements showed excellent performance in forecasting and differentiating growing nGGOs from stable ones (AUC = 0.927,  $P < 0.001$ ), which was better than any CT measurements alone. Besides, the Ki67-PI Prediction was also independent variable that could predict volume doubling time of the growing nGGOs. This noninvasive index may be of great importance to the selection of treatment and evaluation of prognosis for a specific GGO node.

### Conclusion

In this study, we established a prediction model for calculating Ki67 proliferation index of nGGOs based on non-enhanced CT measurements. This index allows for preoperatively estimating the invasiveness, growth and prognosis of nGGOs more accurately from not only radiology but also pathology.

### Acknowledgements

The present study was funded by the General Foundation Program of Health and Family Planning Commission of Hubei Province. (Grant No. JX6B105).

### Disclosure of conflict of interest

None.

**Address correspondence to:** Guangming Li, Department of Radiology, North Part of Xiangyang Central Hospital, No. 1 in Zhongyuan Road, Fancheng District, Xiangyang 441003, Hubei Province, China. Tel: +86-0710-3235093; Fax: +86-0710-3021457; E-mail: ligm188@sina.com; Guilian Yu, Department of Gynecology and Obstetrics, Xiangyang Central Hospital, No. 136 in Jingzhou Street, Xiangcheng District, Xiangyang 441021, Hubei Province, China. E-mail: 503214721@qq.com

### References

- [1] Aberle DR, Adams AM, Berg CD, Black WC, Clapp JD, Fagerstrom RM, Gareen IF, Gatsonis C, Marcus PM and Sicks JD. Reduced lung-

## Ki67-PI prediction allows assessing invasiveness and forecasting growth of GGO

- cancer mortality with low-dose computed tomographic screening. *N Engl J Med* 2011; 365: 395-409.
- [2] Zhang L, Yankelevitz DF, Carter D, Henschke CI, Yip R and Reeves AP. Internal growth of non-solid lung nodules: radiologic-pathologic correlation. *Radiology* 2012; 263: 279-286.
- [3] Tamura M, Shimizu Y, Yamamoto T, Yoshikawa J and Hashizume Y. Predictive value of one-dimensional mean computed tomography value of ground-glass opacity on high-resolution images for the possibility of future change. *J Thorac Oncol* 2014; 9: 469-472.
- [4] Naidich DP, Bankier AA, MacMahon H, Schaefer-Prokop CM, Pistolesi M, Goo JM, Macchiarini P, Crapo JD, Herold CJ, Austin JH and Travis WD. Recommendations for the management of subsolid pulmonary nodules detected at CT: a statement from the Fleischner society. *Radiology* 2013; 266: 304-317.
- [5] Kobayashi Y, Fukui T, Ito S, Usami N, Hatooka S, Yatabe Y and Mitsudomi T. How long should small lung lesions of ground-glass opacity be followed? *J Thorac Oncol* 2013; 8: 309-314.
- [6] Lee HY, Choi Y, Lee KS, Han J, Zo JI, Shim YM and Moon JW. Pure ground-glass opacity neoplastic lung nodules: histopathology, imaging, and management. *Am J Roentgenol* 2014; 202: W224-W233.
- [7] Travis WD, Brambilla E, Noguchi M, Nicholson AG, Geisinger K, Yatabe Y, Powell CA, Beer D, Riely G, Garg K, Austin JH, Rusch VW, Hirsch FR, Jett J, Yang PC and Gould M. International Association for the Study Of Lung Cancer/American Thoracic Society/European Respiratory Society: international multidisciplinary classification of lung adenocarcinoma: executive summary. *Proc Am Thorac Soc* 2011; 8: 381-385.
- [8] Min JH, Lee HY, Lee KS, Han J, Park K, Ahn MJ and Lee SJ. Stepwise evolution from a focal pure pulmonary ground-glass opacity nodule into an invasive lung adenocarcinoma: an observation for more than 10 years. *Lung Cancer* 2010; 69: 123-126.
- [9] Jin X, Zhao S, Gao J, Wang D, Wu J, Wu C, Chang R and Ju H. CT characteristics and pathological implications of early stage (t1n0m0) lung adenocarcinoma with pure ground-glass opacity. *Eur Radiol* 2015; 25: 2532-2540.
- [10] Son JY, Lee HY, Lee KS, Kim J, Han J, Jeong JY, Kwon OJ and Shim YM. Quantitative CT analysis of pulmonary ground-glass opacity nodules for the distinction of invasive adenocarcinoma from pre-invasive or minimally invasive adenocarcinoma. *PLoS One* 2014; 9: e104066.
- [11] de Hoop B, Gietema H, van de Vorst S, Murphy K, van Klaveren RJ and Prokop M. Pulmonary ground-glass nodules: increase in mass as an early indicator of growth. *Radiology* 2010; 255: 199-206.
- [12] Goo JM, Park CM and Lee HJ. Ground-glass nodules on chest CT as imaging biomarkers in the management of lung adenocarcinoma. *AJR Am J Roentgenol* 2011; 196: 533-543.
- [13] Nakata M, Sawada S, Saeki H, Takashima S, Mogami H, Teramoto N and Eguchi K. Prospective study of thoracoscopic limited resection for ground-glass opacity selected by computed tomography. *Ann Thorac Surg* 2003; 75: 1601-1606.
- [14] Ji Y, Zheng M, Ye S, Chen J and Chen Y. PTEN and Ki67 expression is associated with clinicopathologic features of non-small cell lung cancer. *J Biomed Res* 2014; 28: 462-467.
- [15] Berghoff AS, Ilhan-Mutlu A, Wöhrer A, Hackl M, Widhalm G, Hainfellner JA, Dieckmann K, Melchardt T, Dome B, Heinzl H, Birner P and Preusser M. Prognostic significance of Ki67 proliferation index, HIF1 alpha index and microvascular density in patients with non-small cell lung cancer brain metastases. *Strahlenther Onkol* 2014; 190: 676-685.
- [16] Ciancio N, Galasso MG, Campisi R, Bivona L, Migliore M and Di Maria GU. Prognostic value of p53 and Ki67 expression in fiberoptic bronchial biopsies of patients with non small cell lung cancer. *Multidiscip Respir Med* 2012; 7: 29.
- [17] Peng M, Peng F, Zhang C, Wang Q, Li Z, Hu H, Liu S, Xu B, Zhu W, Han Y and Lin Q. Preoperative prediction of Ki-67 labeling index by three-dimensional ct image parameters for differential diagnosis of ground-glass opacity (GGO). *PLoS One* 2015; 10: e129206.
- [18] Hansell DM, Bankier AA, MacMahon H, McLoud TC, Muller NL and Remy J. Fleischner society: glossary of terms for thoracic imaging. *Radiology* 2008; 246: 697-722.
- [19] Liang M, Liu X, Li W, Li K, Chen X, Wang G, Chen K and Zhang J. Evaluating the growth of pulmonary nodular ground-glass opacity on CT: comparison of volume rendering and thin slice images. *J Huazhong Univ Sci Technolog Med Sci* 2011; 31: 846-851.
- [20] Sone S, Nakayama T, Honda T, Tsushima K, Li F, Haniuda M, Takahashi Y, Suzuki T, Yamanda T, Kondo R, Hanaoka T, Takayama F, Kubo K and Fushimi H. Long-term follow-up study of a population-based 1996-1998 mass screening programme for lung cancer using mobile low-dose spiral computed tomography. *Lung Cancer* 2007; 58: 329-341.
- [21] Wang CJ, Zhou ZG, Holmqvist A, Zhang H, Li Y, Adell G and Sun XF. Survivin expression quantified by image pro-plus compared with visual assessment. *Appl Immunohistochem Mol Morphol* 2009; 17: 530-535.

## Ki67-PI prediction allows assessing invasiveness and forecasting growth of GGO

- [22] Francisco JS, Moraes HP and Dias EP. Evaluation of the image-pro plus 4.5 software for automatic counting of labeled nuclei by pcna immunohistochemistry. *Braz Oral Res* 2004; 18: 100-104.
- [23] Busing KA, Kilian AK, Schaible T, Debus A, Weiss C and Neff KW. Reliability and validity of mr image lung volume measurement in fetuses with congenital diaphragmatic hernia and in vitro lung models. *Radiology* 2008; 246: 553-561.
- [24] Sergiacomi G, Ciccio C, Boi L, Velari L, Crusco S, Orlacchio A and Simonetti G. Ground-glass opacity: high-resolution computed tomography and 64-multi-slice computed tomography findings comparison. *Eur J Radiol* 2010; 74: 479-483.
- [25] DeLong ER, DeLong DM and Clarke-Pearson DL. Comparing the areas under two or more correlated receiver operating characteristic curves: a nonparametric approach. *Biometrics* 1988; 44: 837-845.
- [26] Kostis WJ, Yankelevitz DF, Reeves AP, Fluturo SC and Henschke CI. Small pulmonary nodules: reproducibility of three-dimensional volumetric measurement and estimation of time to follow-up CT. *Radiology* 2004; 231: 446-452.
- [27] Tamura M, Shimizu Y, Yamamoto T, Yoshikawa J and Hashizume Y. Predictive value of one-dimensional mean computed tomography value of ground-glass opacity on high-resolution images for the possibility of future change. *J Thorac Oncol* 2014; 9: 469-472.
- [28] Bak SH, Lee HY, Kim JH, Um SW, Kwon OJ, Han J, Kim HK, Kim J and Lee KS. Quantitative CT analysis of pure ground-glass opacity nodule (GGN) predicts further ct change. *Chest* 2016; 149: 180-191.
- [29] Takahashi M, Shigematsu Y, Ohta M, Tokumasu H, Matsukura T and Hirai T. Tumor invasiveness as defined by the newly proposed IASLC/ATS/ERS classification has prognostic significance for pathologic stage IA lung adenocarcinoma and can be predicted by radiologic parameters. *J Thorac Cardiovasc Surg* 2014; 147: 54-59.
- [30] Scholzen T and Gerdes J. The Ki-67 protein: from the known and the unknown. *J Cell Physiol* 2000; 182: 311-322.
- [31] Park CM, Goo JM, Lee HJ, Lee CH, Chun EJ and Im JG. Nodular ground-glass opacity at thin-section CT: histologic correlation and evaluation of change at follow-up. *Radiographics* 2007; 27: 391-408.
- [32] El-Sherief AH, Gilman MD, Healey TT, Tambouret RH, Shepard JA, Abbott GF and Wu CC. Clear vision through the haze: a practical approach to ground-glass opacity. *Curr Probl Diagn Radiol* 2014; 43: 140-158.
- [33] Henschke CI, Yankelevitz DF, Mirtcheva R, McGuinness G, McCauley D and Miettinen OS. CT screening for lung cancer: frequency and significance of part-solid and nonsolid nodules. *AJR Am J Roentgenol* 2002; 178: 1053-1057.
- [34] Koo CW, Miller WT and Kucharczuk JC. Focal ground-glass opacities in non-small cell lung carcinoma resection patients. *Eur J Radiol* 2012; 81: 139-145.